

Search for Scalar Diquarks at the LHeC Based Gamma-Proton Collider

M. Şahin^a and O. Çakır^b

Physics Department, Faculty of Sciences, Ankara University,
06100, Tandoğan, Ankara, Turkey

^asahinm@science.ankara.edu.tr

^bocakir@science.ankara.edu.tr

November 1, 2018

Abstract

The diquark exotics which couple to a pair of quarks are predicted by the Compositeness and Superstring inspired E_6 model. We study the single production of scalar diquarks at LHeC based γp collider options. The background for three jet final states are examined through appropriate kinematical cuts. We discuss the possibility of measurements for the charges of scalar diquarks (qq and qq').

1. Introduction

Diquarks are suggested by the models beyond the Standard Model (SM), such as the superstring-inspired E_6 models [1] and composite models [2]. Diquarks have scalar and vector form and carry baryon number $|B| = 2/3$, and no lepton number. They carry electric charges $|Q| = 1/3, 2/3$ or $4/3$.

Diquark production was examined in hadron colliders $p\bar{p}/pp$ [3, 4, 5, 6, 7, 8, 9], e^-e^+ [6, 10] and ep colliders [6, 11]. The collider dedector at Fermilab (CDF) has set limits on the masses of scalar

Table 1: Main parameters of energy and luminosity options of LHeC based γp collider.

Collider	E_e (TeV)	E_p (TeV)	$\sqrt{s_{ep}}$ (TeV)	$\sqrt{s_{\gamma p}^{max}}$	$L_{\gamma p}^{int} L_{ep}^{int} (10^2 pb^{-1})$
LHeC	0.07	7	1.40	1.28	10-100
LHeC	0.14	7	1.98	1.80	10-100

diquarks (predicted by E_6 model) decaying to dijets with the exclusion of mass range $290 < m_{DQ} < 630$ GeV [3]. This limit is expected to be approximately valid for other scalar diquarks. There is also indirect bounds imposed on couplings by the electroweak precision data from LEP where these bounds allow diquark-quark couplings up to a value $\alpha_{DQ}=0.12$ [12].

In this work, we analysed single production of scalar diquarks in a LHeC based γp collider. Interaction Lagrangian and quantum numbers of scalar diquarks are examined to calculate the decay widths, differential cross sections and total cross sections of the signal, and the corresponding background. The signal and background analysis are performed for the scalar diquarks of uu , ud and dd types. The main parameters of the energy and luminosity options for a LHeC based γp collider are listed in table (1).

2. Interaction Lagrangian

Model independent, baryon number conserving, general $SU(3)_C \times SU(2)_W \times U(1)_Y$ invariant effective lagrangian for scalar and vector diquarks has the form [4, 5]

$$\begin{aligned}
L_{|B|=2/3} = & (g_{1L}\bar{q}_L^c i\tau_2 q_L + g_{1R}\bar{u}_R^c d_R)DQ_1^c + \tilde{g}_{1R}\bar{d}_R^c d_R \widetilde{DQ}_1^c \\
& + \tilde{g}'_{1R}\bar{u}_R^c u_R \widetilde{DQ}'_1^c + g_{3L}\bar{q}_R^c i\tau_2 \tau q_L \cdot \mathbf{DQ}_3^c \\
& + g_2\bar{q}_L^c \gamma_\mu d_R DQ_{2\mu}^c + \tilde{g}_2\bar{q}_L^c \gamma^\mu u_R \widetilde{DQ}_{2\mu}^c + H.c.
\end{aligned} \tag{1}$$

In Eq. (1), $q_L = (u_L, d_L)$ denotes the left-handed quark spinor and $q^c = Cq^T$ ($\bar{q}^c = -q^T C^{-1}$) is the charge conjugated quark field. For the sake of simplicity, color and generation indices are omitted in (1). Scalar diquarks DQ_1 , \widetilde{DQ}_1 , \widetilde{DQ}'_1 are $SU(2)_W$ singlets and \mathbf{DQ}_3 is a $SU(2)_W$ triplet. Vector diquarks DQ_2 and \widetilde{DQ}_2 are $SU(2)_W$

Table 2: Quantum numbers of the first generation, color anti-triplet diquarks described by the effective lagrangian (1).

	SU(3) _C	SU(2) _W	U(1) _Y	Q	Couplings
Scalar Diquarks					
DQ_1	$\mathbf{3}^*$	1	2/3	1/3	$u_L d_L(g_{1L}), u_R d_R(g_{1R})$
\widetilde{DQ}_1	$\mathbf{3}^*$	1	-4/3	2/3	$d_R d_R(\tilde{g}_{1R})$
\widetilde{DQ}'_1	$\mathbf{3}^*$	1	8/3	4/3	$u_R u_R(\tilde{g}'_{1R})$
DQ_3	$\mathbf{3}^*$	3	2/3	$\begin{pmatrix} 4/3 \\ 1/3 \\ -2/3 \end{pmatrix}$	$\begin{pmatrix} u_L u_L(\sqrt{2}g_{3L}) \\ u_L d_L(-g_{3L}) \\ d_L d_L(-\sqrt{2}g_{3L}) \end{pmatrix}$
Vector Diquarks					
$DQ_{2\mu}$	$\mathbf{3}^*$	2	-1/3	$\begin{pmatrix} 1/3 \\ -2/3 \end{pmatrix}$	$\begin{pmatrix} d_R u_L(g_2) \\ d_R d_L(-g_2) \end{pmatrix}$
$\widetilde{DQ}_{2\mu}$	$\mathbf{3}^*$	2	5/3	$\begin{pmatrix} 4/3 \\ 1/3 \end{pmatrix}$	$\begin{pmatrix} u_R u_L(\tilde{g}_2) \\ u_R d_L(-\tilde{g}_2) \end{pmatrix}$

doublets. At this stage, we assume that each SM generation has its own diquarks and relevant couplings in order to avoid flavour changing neutral currents. A general classification of the first generation, color anti-triplet ($\mathbf{3}^*$) diquarks is shown in table 1 [6].

We consider the color $\mathbf{3}^*$ scalar DQ_1 or DQ_3^0 diquarks coupled to ud pairs, \widetilde{DQ}_1 or DQ_3^- diquarks coupled to dd pair and \widetilde{DQ}'_1 or DQ_3^+ diquarks coupled to uu pair. Here, $DQ_3^{(+,0,-)}$ denotes the isospin triplet component of scalar diquarks. Diquark interactions with the gauge bosons are given as

$$L = \sum_{\Phi=DQ_i} (D_\mu \Phi)^\dagger (D^\mu \Phi) - M_\Phi^2 \Phi^\dagger \Phi \quad (2)$$

where covariant derivative is $D_\mu = \partial_\mu - ig_e Q_{DQ} A_\mu - ig_e Q^Z Z_\mu - ig_e Q^W W_\mu - ig_s \frac{\lambda_a}{2} G_\mu^a$ where A_μ , Z_μ , W_μ and G_μ^a denote photon, Z -boson, W -boson and gluon fields, respectively. Q_{DQ} is the electromagnetic charge of a given diquark DQ and $Q^Z = (T_3 - Q_{DQ} \sin^2 \theta_W) / (\cos \theta_W \sin \theta_W)$ is the weak charge, T_3 the third component of the weak isospin and θ_W is the Weinberg angle, g_s is the strong coupling constant and λ_a are the Gell-Mann matrices.

The decay widths (Γ_{DQ}) for scalar diquark is calculated from the equation (1) and we plot the diquark decay width versus diquark mass in fig. 1.

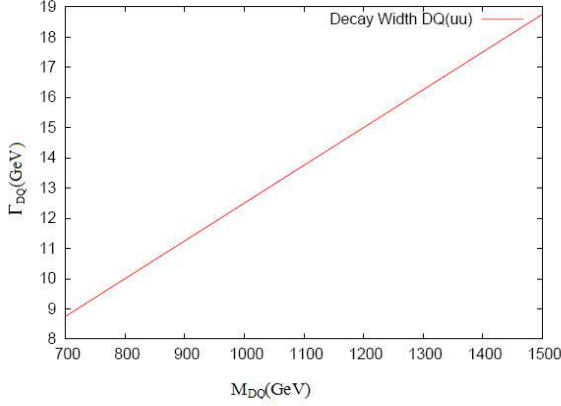


Figure 1: Decay width versus mass for scalar diquark $DQ(uu)$.

3. Production Cross Section for Scalar Diquarks

Scalar diquarks can be produced singly via the subprocess $\gamma p \rightarrow q' DQ$ and the differential cross section is given by

$$\begin{aligned}
\frac{d\hat{\sigma}_S}{d\hat{t}} = & \frac{g_e^2 g_{DQ}^2}{16\pi \hat{s}^2} \left[\frac{Q'^2 \hat{s}}{(\hat{s} + \hat{t} - m_{DQ}^2)} - \frac{2QQ'(\hat{s} + \hat{t})(\hat{s} - m_{DQ}^2)}{\hat{s}(\hat{s} + \hat{t} - m_{DQ}^2)} \right. \\
& + \frac{Q^2(\hat{s} + \hat{t} - m_{DQ}^2)}{\hat{s}} - \frac{Q_{DQ}Q\hat{t}(\hat{s} - 2m_{DQ}^2)(\hat{t} - m_{DQ}^2)}{\hat{s}(\hat{t}^2 + \Gamma_{DQ}^2 m_{DQ}^2 - 2\hat{t}m_{DQ}^2 + m_{DQ}^4)} \\
& \quad + \frac{Q_{DQ}^2 \hat{t}(\hat{t} + m_{DQ}^2)}{(\hat{t}^2 + \Gamma_{DQ}^2 m_{DQ}^2 - 2\hat{t}m_{DQ}^2 + m_{DQ}^4)} \\
& \quad \left. + \frac{Q_{DQ}Q'\hat{t}(\hat{t} - m_{DQ}^2)((\hat{s} + \hat{t} + m_{DQ}^2))}{(\hat{s} + \hat{t} - m_{DQ}^2)(\hat{t}^2 + \Gamma_{DQ}^2 m_{DQ}^2 - 2\hat{t}m_{DQ}^2 + m_{DQ}^4)} \right] \quad (3)
\end{aligned}$$

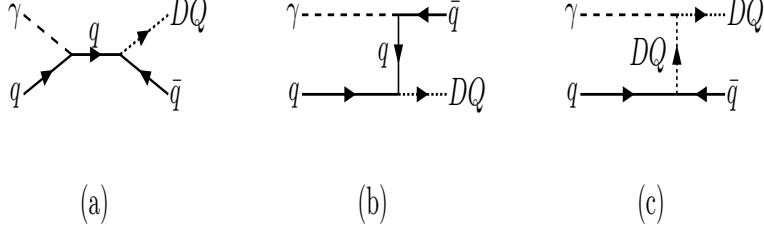


Figure 2: Diagrams for the single production of scalar diquarks at LHeC based γp collider.

where \hat{s} and \hat{t} are Mandelstam variables for the subprocess $\gamma q \rightarrow DQq'$. Q and Q' are the charges of initial and final quarks, respectively. As it can be seen from equation (3), the cross section is proportional to diquark charges. Therefore, the diquark charges can be identified at a LHeC based γp collider. In figure 2, the hadronic process for diquark single production is shown.

The signal for diquark single production would clearly manifest itself in three jets cross sections. The total cross section for the single production of diquarks at γp collider is given by

$$\sigma_{DQ}^S = \sum_q \int_{M_{DQ}^2/s}^{0.83} d\tau \int_{\tau/0.83}^1 \frac{dx}{x} f_{q/p}(x, Q^2) f_{\gamma/e}\left(\frac{\tau}{x}\right) \int_{\hat{t}_{\min}}^{\hat{t}_{\max}} dt \frac{d\hat{\sigma}_{DQ}^S}{dt} \quad (4)$$

where $f_q(x, Q^2)$ is the quark distribution functions from the proton. The third integration over \hat{t} is taken in the interval \hat{t}_{\min} and \hat{t}_{\max} , where $\hat{t}_{\min} = -\hat{s} + m_{DQ}^2$ and $\hat{t}_{\max} = 0$. The energy spectrum of the Compton backscattered photons from electrons is given by

$$f_{\gamma/e}(z) = \frac{1}{D(\xi)} \left[1 - z + \frac{1}{1-z} - \frac{4z}{\xi(1-z)} + \frac{4z^2}{\xi^2(1-z)^2} \right], \quad (5)$$

with

$$D(\xi) = \left(\frac{1}{2} + \frac{8}{\xi} - \frac{1}{2(1+\xi)^2} \right) + \left(1 - \frac{4}{\xi} - \frac{8}{\xi^2} \right) \ln(1+\xi), \quad (6)$$

where $\xi = 4E_e\omega_0/m_e^2$, and $z = E_\gamma/E_e$ is the ratio of the backscattered photon energy to the initial electron energy. The energy E_γ of

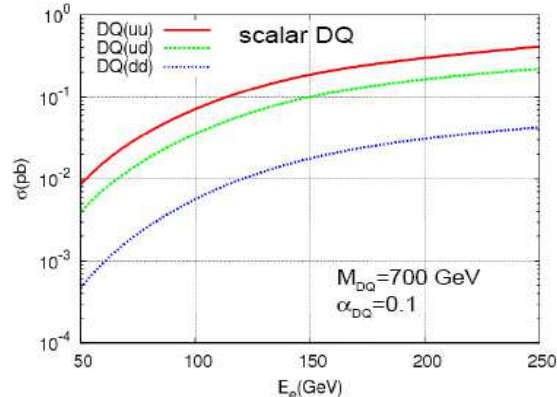


Figure 3: Total cross sections for single scalar diquark ($m_{DQ} = 700$ GeV) production as a function of the electron beam energy ($E_e = 50 - 250$ GeV) at ep colliders, where proton beam (from the LHC) has an energy $E_p = 7000$ GeV.

converted photons restricted by the condition $z_{\max} = 0.83$. The value $z_{\max} = \xi/(\xi + 1) = 0.83$ corresponds to $\xi = 4.8$ as given in [13].

In figure 3, total cross sections for scalar diquarks depending on the electron beam energies are shown. From these plots we see the high energy and low energy behaviour of the total cross section for a given value of m_{DQ} and α_{DQ} . The total cross sections have no divergencies at large energies. Thus, equation (4) prove the unitarity condition. In figure (4), the total cross sections versus scalar diquark masses are plotted for the LHeC ($\sqrt{s} = 1.4$ TeV) energy with the coupling $\alpha_{DQ} = 0.1$ using CTEQ parton distribution functions [14] at the factorization scale $Q^2 = m_{DQ}^2$. From these figures we find that diquarks with charge $|Q| = 4/3$ have the largest cross sections when compared to the other types.

4. Signal and Background

We generate diquark signal and the corresponding background events with the program CalcHEP [15]. Here, we consider two types of background one is interfering with the signal events and the other is re-

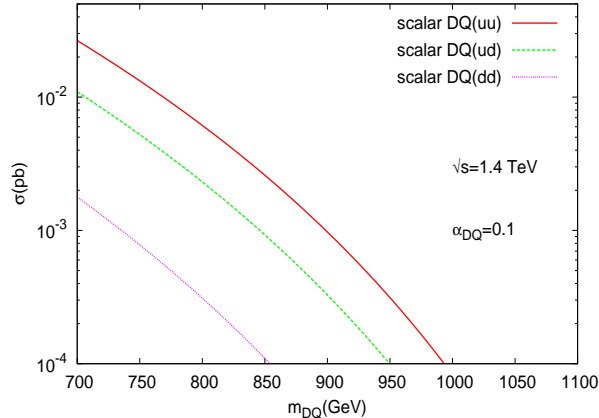


Figure 4: Total cross sections as a function of scalar diquark masses at LHeC with $\sqrt{s} = 1.4$ TeV.

ducible background contributing to three-jet events. The background for three-jet events have large cross sections, since the signal has different shape than the background, still we have opportunity to reduce these backgrounds by applying suitable kinematical cuts. In figure (5), the p_T distribution of 3 jets for signal with $M_{DQ} = 700$ GeV are shown. The jets from diquarks have large transverse momentum distribution around the half value of the diquark mass. Thus, we need at least 20 GeV for the transverse momentum cut and additional kinematics variables to reduce background more efficiently. In figure (6), the pseudo-rapidity distribution for signal with $M_{DQ} = 700$ GeV and background are shown at LHeC with $\sqrt{s} = 1.4$ TeV.

From figure (6), signal jets from scalar diquark are mostly located in the pseudo-rapidity (η) region $1 < \eta < 3.2$. In figure (7), one can see the distribution of pseudo-rapidity (mostly in the range $1 < \eta < 2$) from SM three-jet background at LHeC with $\sqrt{s} = 1.4$ TeV. The invariant mass distribution of dijets from the scalar diquark signal and the SM background are shown in figure (8).

From these figures, more appropriate cuts for signal jets are $1 < \eta^j < 3.2$, $m_{DQ} - \Delta m < m_{jj} < m_{DQ} + \Delta m$, $p_T^j > 20$ GeV at LHeC $\sqrt{s} = 1.4$ TeV energy option. Same calculations have been performed for LHeC $\sqrt{s} = 1.96$ TeV energy option. In this case, the appropriate cuts for signal jets has been founded as $-0.5 < \eta^j < 3$, $m_{DQ} - \Delta m <$

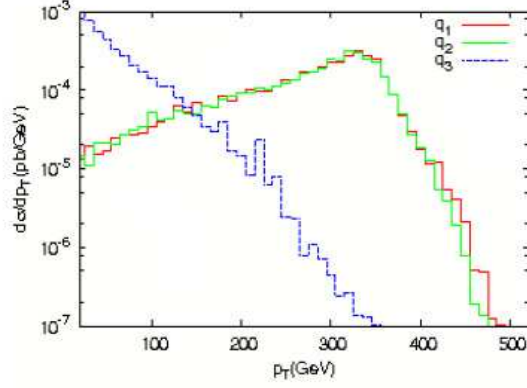


Figure 5: Transverse momentum distributon for scalar diquarks with $M_{DQ} = 700$ GeV at $\sqrt{s} = 1.4$ TeV LHeC energy options.

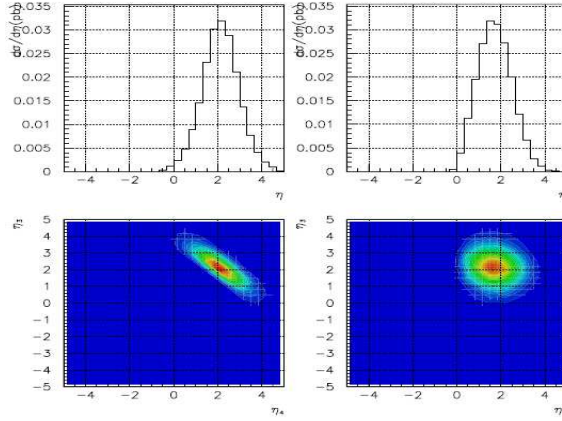


Figure 6: Pseudo-rapidity distribution for the jets from scalar diquark production with $M_{DQ} = 700$ GeV at $\sqrt{s} = 1.4$ TeV LHeC energy option.

$m_{jj} < m_{DQ} + \Delta m, p_T^j > 20$ GeV at LHeC $\sqrt{s} = 1.96$ TeV energy option.

In order to obtain the observability of diquarks at LHeC based gamma-p collider we have calculated the signal (S) and background (B) event estimations for an integrated luminosity of $10^4 pb^{-1}$ for

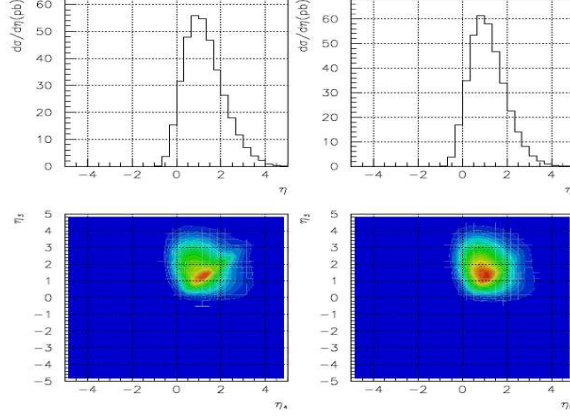


Figure 7: Pseudo-rapidity distributions for SM $3jet$ background at $\sqrt{s} = 1.4$ TeV LHeC energy option.

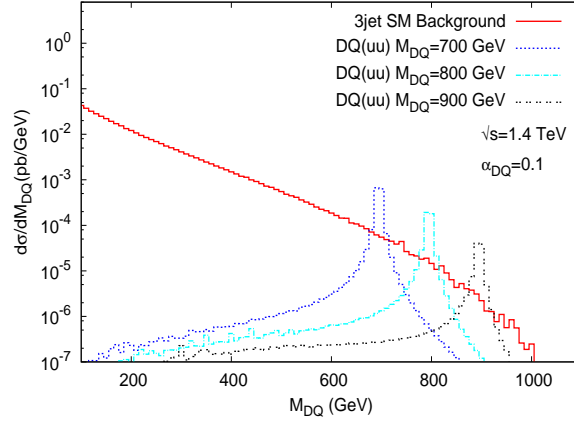


Figure 8: Dijet invariant mass distributions for $ep \rightarrow DQjX \rightarrow jjj$. Resonance peaks are shown for scalar and vector diquark masses 700, 800, 900 GeV for comparison with smooth QCD backgrounds.

one year of operation. The signal generated by a diquark of mass m_{DQ} and decay rate Γ_{DQ} is calculated integrating the differential cross section in the two-jet invariant mass interval $m_{DQ} - \Gamma_{DQ} < m_{jj} < m_{DQ} + \Gamma_{DQ}$ which gives approximately 95% of the events around

Table 3: Observability of diquarks at γp collider based on LHeC $\sqrt{s} = 1.4$ TeV.

	SS for $L_{int} = 10^4 pb^{-1}$		
$M_{DQ}(\text{GeV})$	$DQ(uu)$	$DQ(ud)$	$DQ(dd)$
700	17.2	3.6	1.2
800	10.1	1.8	—
900	4.8	—	—

Table 4: Observability of diquarks at γp collider based on LHeC $\sqrt{s} = 1.98$ TeV.

	SS for $L_{int} = 10^4 pb^{-1}$		
$M_{DQ}(\text{GeV})$	$DQ(uu)$	$DQ(ud)$	$DQ(dd)$
700	36.4	10.8	3.6
800	28.3	7.8	2.5
900	19.9	5.1	1.6
1000	14.9	3.4	1.0
1100	10.4	2.1	—
1200	6.3	—	—

the resonance. For a realistic analysis of the background events we take into account the finite energy resolution of the generic hadronic calorimeter as $\delta E/E = 0.5/\sqrt{E} + 0.03$ for jets with $|y| < 3$. The corresponding two-jet invariant mass resolution is given approximately by $\delta m_{jj} = 0.5\sqrt{m_{jj}} + 0.02m_{jj}$. The background is calculated by integrating the cross sections in the range $m_{DQ} - \Delta m < m_{jj} < m_{DQ} + \Delta m$ with $\Delta m = \max(\Gamma_{DQ}, \delta m_{jj})$. The significance of signal over the background is defined as S/\sqrt{B} . Thus we used appropriate cuts and the detector parameters to find the observability of diquarks at LHeC based γp collider. Then, we listed the values in table (3) and (4) where SS represent significance of diquarks.

If we take at least 10 signal events and $S/\sqrt{B} \geq 3$ as observability criteria, For the diquarks with charge $|Q| = 2/3$ it is possible to cover mass ranges up to 0.8 TeV at the LHeC with $L_{int} = 10^4 pb^{-1}$ and $\sqrt{s} = 1.98$ TeV. The scalar diquarks with charge $|Q| = 4/3$ can be observed up to 1.2 TeV at $\sqrt{s} = 1.98$ TeV.

5. Conclusion

If diquarks exist, LHC could find them in resonance channel, however their charges and coupling types can be identified at a LHeC based γp collider. Up to 1.2 TeV mass of diquarks can be studied at LHeC based γp collider. In the single production mechanism, the spin of the diquarks can also be determined by studying the angular distributions of the final state jets with high p_T .

Acknowledgements

This work is supported in part by the Turkish Atomic Energy Authority (TAEK) and the State Planning Organization (DPT) with grant number DPT2006K-120470.

References

- [1] J. L. Hewett and T. G. Rizzo, Phys. Rep., **183**, 193, 1989.
- [2] H. Terazawa, Phys. Rev. **D22**, 184, 1980.
- [3] CDF Collaboration, CDF note **9246**,2008.
- [4] S. Atag, O. Cakir, and S. Sultansoy,Phys. Rev., **D59**, 015008, 1999.
- [5] E. Arik, S. A. Cetin, O. Cakir and S. Sultansoy, J. High Energy Phys., **09**, 024, 2002.
- [6] O. Cakir, and M. Sahin, Phys. Rev., **D72**, 115011, 2005.
- [7] R.N.Mohapatra, Nobuchika Okada, and Hai-Bo Yu, Phys.Rev. D **77**, 01170(R), 2008.
- [8] M. Sahin, and O. Cakir, Balkan Physics Letters (BPL), **16(1)**, pp. 120-125, 161020 (2009).
- [9] Tao Han, Ian Lewis, and Thomas McElmurry, arXiv:0909.2666v1 [hep-ph] 15 Sep 2009.
- [10] A. Gusso, J. Phys. G:Nucl. Part. Phys. 30 (2004) 691-702.
- [11] T.G. Rizzo, Z.Phys. C **43**, 223, 1989.
- [12] G. Bhattacharyya, D. Choudury and K. Sridhar,Phys. Lett., **B355**,193, 1995.
- [13] G. Bhattacharyya, D. Choudury and K. Sridhar,Phys. Lett., **B355**,193, 1995.
- [14] CTEQ Collaboration, H.L. Lai et al., Eur.Phys. J.**C12** (2000) 375.

- [15] A.Pukhov et al.,**hep-ph/9908288**; A. Pukhov, e-Print Archive, **hep-ph/0412191**, 2004.
- [16] B. Schrempp, **MPI-PAE/PTh**, 72-86, 1986.; W. Buchmuller, Acta Phys. Austriaca,**27**, 517,1985
- [17] H. L. Lai et al. (CTEQ Collaboration), Eur. Phys. J., **C 12**, 375, 2000.
- [18] ATLAS Collaboration, Report No. ATLAS TDR 14, CERN/LHCC 99-14, 1999; Report No. ATLAS TDR 15, CERN/LHCC 99-15, 1999.